Intermediate energy electron impact excitation of composite vibrational modes in phenol

R. F. C. Neves, D. B. Jones, M. C. A. Lopes, K. L. Nixon, E. M. de Oliveira, R. F. da Costa, M. T. do N. Varella, M. H. F. Bettega, M. A. P. Lima, G. B. da Silva, and M. J. Brunger

Citation: The Journal of Chemical Physics **142**, 194302 (2015); doi: 10.1063/1.4921038
View online: http://dx.doi.org/10.1063/1.4921038
View Table of Contents: http://scitation.aip.org/content/aip/journal/jcp/142/19?ver=pdfcov
Published by the AIP Publishing

Intermediate energy electron impact excitation of composite vibrational modes in phenol

R. F. C. Neves,[1,2,3] D. B. Jones,[1] M. C. A. Lopes,[3] K. L. Nixon,[3] E. M. de Oliveira,[4] R. F. da Costa,[5] M. T. do N. Varella,[6] M. H. F. Bettega,[7] M. A. P. Lima,[4] G. B. da Silva,[8] and M. J. Brunger[1,9,a)]

[1]*School of Chemical and Physical Sciences, Flinders University, G.P.O. Box 2100, Adelaide, SA 5001, Australia*
[2]*Instituto Federal do Sul de Minas Gerais, Campus Poços de Caldas, Minas Gerais, Brazil*
[3]*Departamento de Física, Universidade Federal de Juiz de Fora, 36036-900, Juiz de Fora, Minas Gerais, Brazil*
[4]*Instituto de Física 'Gleb Wataghin,' Universidade Estadual de Campinas, 13083-859 Campinas, São Paulo, Brazil*
[5]*Centro de Ciências Naturais e Humanas, Universidade Federal do ABC, 09210-580 Santo André, São Paulo, Brazil*
[6]*Instituto de Física, Universidade de São Paulo, C.P. 66318, 05315-970 São Paulo, Brazil*
[7]*Departamento de Física, Universidade Federal do Paraná, C.P. 19044, 81531-990 Curitiba, Paraná, Brazil*
[8]*Universidade Federal de Mato Grosso, Barra do Garças, Mato Grosso, Brazil*
[9]*Institute of Mathematical Sciences, University of Malaya, 50603 Kuala Lumpur, Malaysia*

(Received 13 March 2015; accepted 30 April 2015; published online 15 May 2015)

We report differential cross section results from an experimental investigation into the electron impact excitation of a number of the low-lying composite (unresolved) vibrational modes in phenol (C_6H_5OH). The measurements were carried out at incident electron energies in the range 15–40 eV and for scattered-electron angles in the range 10–90°. The energy resolution of those measurements was typically ~80 meV. Calculations, using the GAMESS code, were also undertaken with a B3LYP/aug-cc-pVDZ level model chemistry, in order to enable us to assign vibrational modes to the features observed in our energy loss spectra. To the best of our knowledge, the present cross sections are the first to be reported for vibrational excitation of the C_6H_5OH molecule by electron impact. © *2015 AIP Publishing LLC.* [http://dx.doi.org/10.1063/1.4921038]

I. INTRODUCTION

To attain a quantitative understanding of electron transport in phenomena such as gas discharges, low-temperature plasma reactors, and radiation damage in matter, a complete set of cross sections (i.e., the total cross section, momentum transfer cross section, integral cross sections, and differential cross sections (DCSs)) is required for all the relevant open channels (e.g., the elastic channel, rotational and vibrational excitations, discrete electronic-state excitation, ionisation (including dissociative ionisation), dissociative electron attachment (DEA), and neutral dissociation) that pertain to the application in question.[1–7] Of special note, particularly for vibrational excitation and DEA, is when the incident electron is temporarily captured by the target species, leading to the formation of resonances,[8] which can lead to a significant enhancement in the magnitude of the scattering cross sections,[8–11] than would otherwise be the case, and/or promote DEA. Indeed, it is well known that this resonance behaviour plays a lead role in the dynamics driving the electron-initiated processes in some of those applications (e.g., Ref. 12). Recently, however, for the biomolecules tetrahydrofuran (THF)[13,14] and tetrahydrofurfuryl alcohol (THFA),[15] it has been demonstrated that the vibrational excitation cross sections persist in magnitude away from the lower-lying shape resonances at intermediate energies. Further, calculated transport properties (e.g., drift velocity and transverse and longitudinal diffusion coefficients), using a Boltzmann formulation,[4–7] for electrons moving in THF under an applied electric field, were found to be sensitive (with differences of up to 17%)[13,14] to employing a complete or partial vibrational excitation cross section set. Here, the vibrational cross sections differed in terms of both the energy ranges covered and where the cross sections' intensity into open channels was assigned. While this effect would need to be quantified on a molecule by molecule basis, it does illustrate that the study of intermediate energy scattering behaviour should not, in general, be ignored.

Atmospheric plasma treatment of sustainable biomass[16,17] appears to be a promising approach to generate important chemicals such as ethanol and phenol. Phenol (C_6H_5OH) has been identified[18] as a potential target of electron-induced breakdown of lignin (a phenolic-based moiety), and so, it represents an excellent prototype sub-unit for lignin. As noted above, to gain an understanding for the utility of atmospheric plasmas to economically generate bio-fuels and other useful chemicals, plasma simulations incorporating complete cross section data bases are required. As a consequence, we have been studying electron scattering from phenol for which very little data had previously existed. In particular, we have recently reported results for the excited electronic-state spectroscopy of phenol,[19] triple differential cross section experimental and theoretical data for electron-impact ionisation of phenol,[20] elastic and total scattering cross

a)Author to whom correspondence should be addressed. Electronic mail: Michael.Brunger@flinders.edu.au

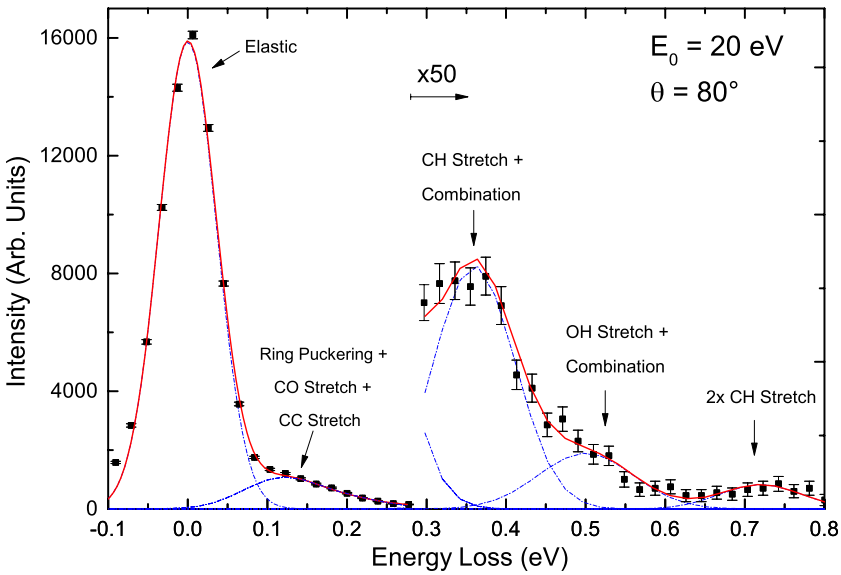

FIG. 1. Typical electron energy loss spectrum of phenol at E_0 = 20 eV, $\theta = 80°$. The overall spectral deconvolution fit is denoted by the solid red line, while the fits to the various vibrational mode features are shown by dashed-dotted blue lines. The features are identified according to their prevalent modes (see also Table I).

sections in phenol[21] and, differential cross sections for electron impact excitation of the discrete electronic-states of phenol.[22] Here, we add to those earlier investigations by reporting on differential cross sections for vibrational excitation of a number of phenol's composite (unresolved) modes up to an energy loss of ~0.8 eV (see Fig. 1).

The structure for the remainder of this paper is as follows. Details of our experimental method, analysis procedures, and quantum chemistry calculations with GAMESS[23] are given in Sec. II, with our results and a discussion of those results then being presented in Sec. III. Finally, in Sec. IV, some concluding remarks will be drawn.

II. EXPERIMENTAL DETAILS, ANALYSIS PROCEDURES AND COMPUTATIONS

An example of a typical electron energy loss spectrum (EELS) measured in the present investigation is given in Fig. 1. Those EELS were acquired with an apparatus based at Flinders University,[24–28] and as it has been discussed many times before only a précis of its functionality is presented here for completeness. A monochromated beam of electrons with energies (E_0) in the range 15–40 eV and a typical current of 1-5 nA was incident on an orthogonal beam of phenol. Our procedures for ensuring a stable beam of phenol (GPR-BOH; >99% assay) into the interaction region were given in Neves *et al.*[22] and so are not repeated again here. Under the stable molecular beam conditions maintained during the EELS measurements, the phenol pressure never exceeded 1×10^{-5} Torr, in the vacuum chamber, in order to minimise the possibility for multiple scattering effects. Note that this was confirmed by measuring the scattered electron signal as a function of pressure, and always working in the region of pressure where a linear dependence is observed. The interaction of the well collimated electron and phenol beams defined a collision volume, and those electrons, which collided with the molecules and were scattered at some angle θ (the electron scattering angle), were energy analysed using a hemispherical selector before being detected with a channel electron multiplier.[24] Note that the angular range of the present EELS was 10° – 90°, while the overall instrumental energy resolution was ~80 meV (FWHM). That energy resolution was insufficient to resolve many of the vibrational modes from one another (see Table I), so that as a consequence, composite vibrational mode DCSs are reported here (see Fig. 1). Energy loss spectra were collected at each θ and E_0 (15, 20, 30, and 40 eV), by recording the number of scattered electrons detected at each energy loss value. The true scattered electron count rate at each energy loss was recorded using a multichannel scaler (MCS) synchronised to a linear voltage ramp that varied the detected energy loss between −0.1 and 0.8 eV. In this way, the EELS are built up by continually scanning over the range of energy loss values, so that the effect of any minor variations in the phenol beam flux or incident electron current on a given energy loss spectrum is minimised. Each EELS was repeatedly measured (2–4 times) to ensure reproducibility of the inelastic to elastic peak ratios (see later) within the experimental uncertainty.

As a part of this study, calculations were performed to derive the optimum phenol geometry and the phenol vibrational normal modes and their frequencies. These computations were performed within a Density Functional Theory (DFT) framework with the hybrid exchange-correlation functional B3LYP and the correlation-consistent aug-cc-pVDZ Gaussian basis set in the GAMESS package,[23] with the results obtained being summarised in Table I. To obtain the optimum geometry, the energy gradient convergence tolerance was set to 10^{-5} Hartree/Bohr. As noted above, with an energy resolution of ~80 meV, many of the allowed modes overlap so that composite modes (see Table I) are experimentally assigned (see also Fig. 1).

The various EELS were then deconvoluted into contributions arising from each composite vibrational feature. In each case, one or two Gaussian functions were used to describe the spectral profile for each resolvable inelastic feature and the elastic scattering peak, with a typical example of the result from such a fit being given in Fig. 1. The best fit to each energy loss spectrum was obtained by allowing the amplitudes of the

TABLE I. Experimentally observed bands and calculated vibrational excitation energies for some of the most IR active vibrational bands of phenol. The calculations were performed at the B3LYP/aug-cc-pVDZ level. These calculations are used to tentatively assign the experimentally observed spectral features.

		B3LYP/aug-cc-pVDZ			
Experimental energy loss (eV)	Experimental assignment	Vibrational mode	Energy (eV)	IR intensity (debye^2/amu. Å^2)	Dominant vibrational mode
0.0	Elastic peak				
		ν_2	0.044	2.266	H-out of plane
		ν_5	0.062	0.380	
0.07–0.30	Ring puckering + CO stretch + CC stretch	ν_8	0.085	0.863	
		ν_9	0.092	1.085	Ring puckering
		ν_{10}	0.099	0.496	
		ν_{20}	0.144	3.202	CO stretch
		ν_{21}	0.153	1.944	
		ν_{23}	0.164	0.567	
		ν_{24}	0.179	0.683	
		ν_{25}	0.182	1.279	CC stretch
		ν_{26}	0.197	1.313	
		ν_{27}	0.198	0.708	
		$2\times\nu_{20}$	0.287		
		$\nu_{20}+\nu_{21}$	0.297		Combination bands
		$2\times\nu_{21}$	0.306		
0.30–0.42	CH stretch + combination	$\nu_{20}+\nu_{25}$	0.326		
		$\nu_{21}+\nu_{25}$	0.335		
		$\nu_{20}+\nu_{26}$	0.341		Combination bands
		$\nu_{21}+\nu_{26}$	0.350		
		$2\times\nu_{25}$	0.364		
		ν_{28}	0.381	0.329	
		ν_{31}	0.384	0.269	CH stretch
		ν_{32}	0.387	0.282	
		$2\times\nu_{26}$	0.394		Overtone band
0.42–0.62	OH stretch + combination	ν_{33}	0.461	1.397	OH stretch
		$\nu_{20}+\nu_{28}$	0.525		
		$\nu_{20}+\nu_{31}$	0.528		Combination bands
		$\nu_{20}+\nu_{32}$	0.531		
		$\nu_{21}+\nu_{28}$	0.534		
0.62–0.80	2×CH stretch	$2\times\nu_{28}$	0.762		
		$2\times\nu_{31}$	0.769		2×CH stretch
		$2\times\nu_{32}$	0.774		

Gaussian functions to vary in a least-squares fitting procedure, whilst holding the peak positions and widths constant. The ratio (R) of the area under the fitting function for each ith composite vibrational feature to that under the elastic peak, at each E_0 and θ, is simply related to the ratio of the differential cross sections (σ) from

$$R_i(E_0,\theta) = \frac{\sigma_i(E_0,\theta)}{\sigma_0(E_0,\theta)}. \quad (1)$$

Note that Eq. (1) is only valid if the transmission efficiency of the analyser remains constant over the energy loss and angular range studied or is at least well characterised. Similar to the technique of Allan,[29] an additional focusing lens (synchronised to the voltage ramp) was also employed to minimise variations in the analyser transmission efficiency for electrons detected with different energy loss values. Of course, in the present measurements, the scattered electron energies (E_{sc}) are all very similar to that for E_0 ($0.95 < \frac{E_{sc}}{E_0} \leqslant 1$), so that a significant transmission effect would not be anticipated. Nonetheless, we place a quite conservative uncertainty of 20% on our efficiency being unity. The present measured R_i for each of the identified (see Fig. 1) composite vibrational modes are summarised in Tables II–V, respectively. It should be transparent from Eq. (1) that the product $R_i \times \sigma_0$ then gives the required composite vibrational DCS, provided the elastic DCS (σ_0) is known. Those results, for the modes in question, can also be found in Tables II–V. In this investigation and in our previous study on the electronic-state DCSs for phenol,[22] we have utilised the benzene elastic DCS from Cho *et al.*[30] and Gulley and Buckman[31] to place our composite vibrational excitation data, at each E_0 and θ, onto an absolute scale. The

TABLE II. Present experimental vibrational-to-elastic ratios ($\times 10^{-3}$), differential cross sections ($\times 10^{-23}$ m^2/sr), and related uncertainty (%) for electron-impact excitation of the phenol ring puckering + CO stretch + CC stretch, 1st vibrational band, (0.07–0.30 eV).

	15 eV			20 eV			30 eV			40 eV		
θ (°)	Ratio	DCS	Uncertainty	Ratio	DCS	Uncertainty	Ratio	DCS	Uncertainty	Ratio	DCS	Uncertainty
10	…	…	…	5.50	751.42	59	4.01	279.82	55	4.10	288.32	56
15	…	…	…	9.07	315.91	59	3.96	129.76	61	5.25	138.23	67
20	25.23	681.75	38	8.41	155.16	61	5.01	71.48	61	8.86	82.15	73
30	156.87	1226.38	25	78.34	343.93	24	69.65	173.28	26	42.88	68.36	74
40	386.53	743.69	26	61.17	67.47	24	75.04	77.37	30	53.48	51.13	44
50	425.81	376.42	22	91.08	60.57	23	75.32	67.49	30	78.31	72.52	26
60	514.32	447.46	22	84.30	69.63	23	74.76	61.98	27	77.17	46.53	67
70	386.70	405.64	24	92.09	83.16	22	94.96	59.06	22	66.73	25.29	22
80	419.25	501.00	21	102.88	85.80	23	101.09	48.32	22	92.81	31.18	24
90	358.31	424.95	22	131.09	93.73	24	164.53	70.91	33	218.36	80.36	31

TABLE III. Present experimental vibrational-to-elastic ratios ($\times 10^{-3}$), differential cross sections ($\times 10^{-23}$ m^2/sr), and related uncertainty (%) for electron-impact excitation of the phenol CH stretch + combination, 2nd vibrational band, (0.30–0.42 eV).

	15 eV			20 eV			30 eV			40 eV		
θ (°)	Ratio	DCS	Uncertainty	Ratio	DCS	Uncertainty	Ratio	DCS	Uncertainty	Ratio	DCS	Uncertainty
10	…	…	…	0.54	74.01	38	0.28	19.84	58	0.38	26.50	65
15	…	…	…	1.01	35.25	28	0.46	15.19	39	0.46	12.21	60
20	8.20	221.53	35	1.53	28.30	31	0.67	9.60	30	0.99	9.13	46
30	60.85	475.72	28	12.96	56.91	24	5.89	14.65	30	5.39	8.59	32
40	184.69	355.34	28	11.39	12.56	23	4.82	4.97	28	5.54	5.30	46
50	133.73	118.21	22	15.77	10.48	24	4.17	3.74	25	5.22	4.84	28
60	169.02	147.04	21	11.66	9.63	23	4.39	3.64	30	5.97	3.60	28
70	156.13	163.78	26	12.59	11.37	24	6.67	4.15	30	7.23	2.74	25
80	175.39	209.59	21	13.58	11.32	23	6.32	3.02	26	7.35	2.47	25
90	142.80	169.37	23	15.52	11.10	25	8.03	3.46	30	11.10	4.08	24

TABLE IV. Present experimental vibrational-to-elastic ratios ($\times 10^{-3}$), differential cross sections ($\times 10^{-23}$ m^2/sr), and related uncertainty (%) for electron-impact excitation of phenol OH stretch + combination, 3rd vibrational band, (0.42–0.62 eV).

	15 eV			20 eV			30 eV			40 eV		
θ (°)	Ratio	DCS	Uncertainty	Ratio	DCS	Uncertainty	Ratio	DCS	Uncertainty	Ratio	DCS	Uncertainty
10	…	…	…	0.25	33.49	30	0.20	14.24	69	0.13	8.95	74
15	…	…	…	0.43	15.13	53	0.10	3.42	72	0.09	2.35	75
20	2.02	54.61	33	0.42	7.66	52	0.17	2.44	71	0.18	1.64	75
30	20.44	159.77	31	4.70	20.61	26	0.50	1.23	81	1.04	1.66	74
40	30.13	57.98	24	1.64	1.81	56	0.50	0.52	74	0.71	0.68	79
50	40.16	35.51	24	2.16	1.44	64	0.61	0.55	60	0.38	0.36	77
60	84.11	73.17	25	2.82	2.33	41	0.65	0.54	71	0.71	0.43	75
70	60.31	63.26	22	3.36	3.04	42	0.77	0.48	74	0.85	0.32	75
80	59.08	70.60	22	3.58	2.99	29	1.32	0.63	63	1.09	0.37	66
90	48.47	57.49	23	4.78	3.42	33	1.53	0.66	44	0.83	0.31	69

efficacy and accuracy of such a choice was recently addressed in detail by da Costa *et al.*[21] and so, we do not repeat that argument here. Suffice it to say, at each of 15 eV, 20 eV, 30 eV, and 40 eV, the phenol elastic Schwinger Multichannel (SMC) differential cross sections were generally found to be in very good agreement with the corresponding elastic benzene measurements,[30,31] in terms of both their shapes and absolute values. Thus, we could have equally well used the elastic phenol results of da Costa *et al.*[21] to effect the normalisation in this case. Note that on the basis of comparing our 1-channel SMC elastic DCSs for benzene and phenol, we estimate on average that an uncertainty of less than 6% is introduced by our normalisation choice.

The present vibrational excitation DCSs for the ring puckering plus CO stretch plus CC stretch, CH stretch plus combination, OH stretch plus combination, and 2 × CH stretch overtone modes are, respectively, given in Tables II–V. Error estimates on those data are also given in each of those

TABLE V. Present experimental vibrational-to-elastic ratios ($\times 10^{-3}$), differential cross sections ($\times 10^{-23}$ m^2/sr), and related uncertainty (%) for electron-impact excitation of phenol 2×CH stretch, 4th vibrational band, (0.62–0.80 eV).

	15 eV			20 eV			30 eV			40 eV		
θ (°)	Ratio	DCS	Uncertainty	Ratio	DCS	Uncertainty	Ratio	DCS	Uncertainty	Ratio	DCS	Uncertainty
10	…	…	…	0.13	17.10	56	0.06	4.01	85	0.11	7.79	81
15	…	…	…	0.20	7.00	83	0.11	3.63	76	0.06	1.64	75
20	1.94	52.45	32	0.17	3.11	72	0.08	1.10	90	0.10	0.96	78
30	13.39	104.69	33	1.37	6.02	34	0.49	1.22	98	0.59	0.95	77
40	38.18	73.46	27	0.75	0.83	81	0.34	0.35	74	0.61	0.59	79
50	35.44	31.33	26	1.18	0.78	74	0.32	0.28	90	0.31	0.29	78
60	57.76	50.25	24	1.00	0.83	73	0.39	0.32	78	0.36	0.22	74
70	51.35	53.86	24	1.13	1.02	61	0.47	0.29	78	0.43	0.16	74
80	50.60	60.47	22	1.16	0.97	57	0.77	0.37	69	0.49	0.16	79
90	44.21	52.44	32	1.36	0.97	62	0.84	0.36	55	0.83	0.31	75

tables. Attention to the identification and quantification of all possible sources of error has been made throughout this study, including the uncertainties, at each E_0 and θ, on the elastic DCS measurements[30,31] used to normalise our measured ratios (see Eq. (1)). When all those factors are combined in quadrature, the errors on our DCS (see Tables II–V) are usually found to be in the range 21–90%, with the largest errors being for the 2 × CH stretch mode for which the statistics were poorer due to its much smaller excitation probability (see Fig. 1). Our excitation DCSs, for each of the modes, are also plotted in Figs. 2–4.

III. RESULTS AND DISCUSSION

In Tables II–V and Figs. 2–4, we present the differential cross section results, for electron impact excitation of the composite vibrational modes from our experimental investigations. It should be immediately apparent from Figs. 2–4 that there are no other measured or calculated DCS against which we might compare the present data. Note that the error bars plotted on each of those figures are at the one standard deviation confidence interval.

Let us now consider Fig. 2 in more detail. Here, we observe that while at 15 eV, the angular distribution (shape) of the DCS is quasi-isotropic; at 20, 30, and 40 eV, the angular distribution does become somewhat more forward peaked in magnitude (note the y-axis log-scale) as you go to smaller scattered electron angles. This latter observation is consistent with either (or both) the permanent dipole moment of phenol ($\mu \sim 1.33$ D[32]) or its dipole polarisability ($\alpha \sim 10.53$ Å^3 [18,20]) starting to play more of a role in the collision dynamics at those higher energies. The quasi-isotropic angular behaviour at 15 eV was also observed previously by us in the vibrational excitation DCS of THF[14] and α-tetrahydrofurfuryl alcohol[15] and so is by no means unique. However, a definitive explanation for this behaviour awaits detailed theoretical calculations on this system, although we do not underestimate for one moment the difficulty of such computations which would require the fixed-nuclei approximation to be abandoned and nuclear dynamics to be explicitly incorporated. All the data embodied in Fig. 2 for the unresolved ring puckering + CO stretch + CC stretch modes are listed in Table II.

If we were to measure the infrared (IR) absorption spectrum of phenol with an appropriate spectrophotometer,[32]

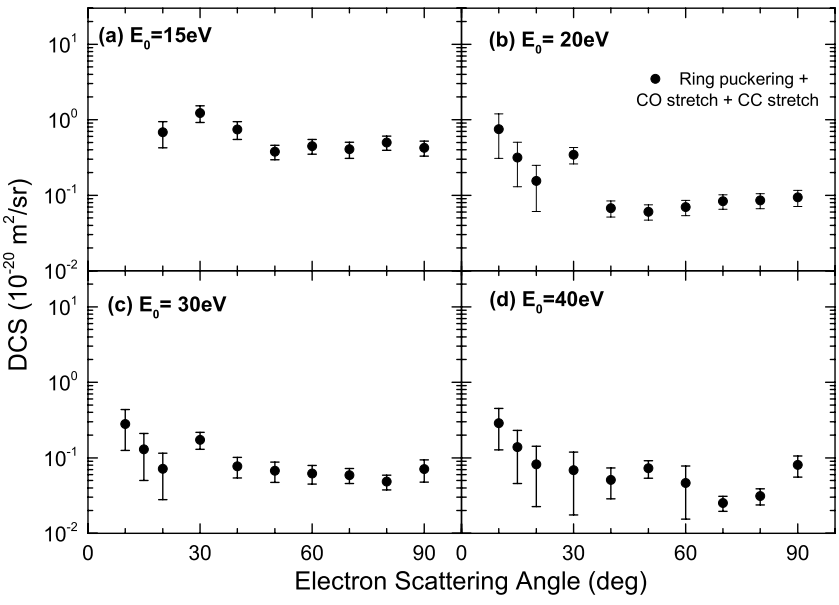

FIG. 2. Differential cross sections ($\times 10^{-20}$ m^2/sr) for electron impact excitation of the unresolved ring puckering, CO stretch and CC stretch modes (•) of phenol at various incident electron energies: (a) 15 eV, (b) 20 eV, (c) 30 eV, and (d) 40 eV. The energy loss range of these modes is 0.07–0.30 eV (see Fig. 1).

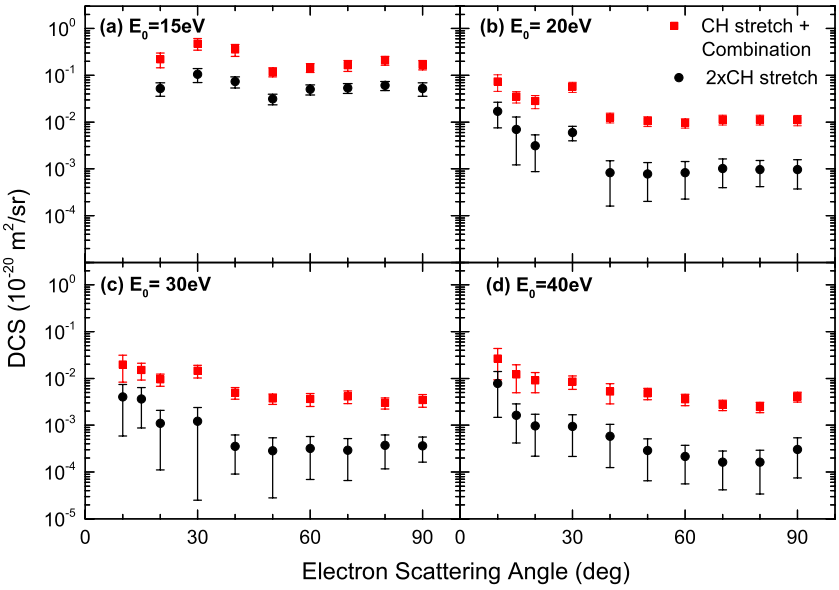

FIG. 3. Differential cross sections ($\times 10^{-20}$ m^2/sr) for electron impact excitation of the unresolved CH stretch and combination modes ("red square") and CH overtone mode (•) of phenol at various incident electrons energies: (a) 15 eV, (b) 20 eV, (c) 30 eV, and (d) 40 eV. The respective energy loss ranges of these modes are 0.30–0.42 eV and 0.62–0.80 eV (see Fig. 1).

then because the relevant potential surfaces are not particularly anharmonic, we would find that the intensity of the fundamental modes is significantly greater than their overtones and also much greater compared to the various possible combination bands. The results plotted in Fig. 3, for both the electron excited CH stretch + combination modes and the $2\times$CH stretch overtone mode, are found to be largely consistent with what one would have expected on the basis of the photon absorption data; namely, because the angular distributions of both the unresolved CH stretch + combination band and the overtone $2\times$CH stretch band are so similar, we might infer that the contribution of the combination modes to the fundamental CH stretch is relatively minor. In addition, it is clear that the magnitude of the CH stretch fundamental is significantly greater than that found for the $2\times$CH stretch overtone. All the cross sections embodied in Fig. 3 for the unresolved CH stretch + combination bands are listed in Table III, while all the data for the $2\times$CH stretch overtone can be found in Table V. Similar to that just described above for the composite modes of Fig. 2, in Fig. 3, we again observe a quasi-isotropic angular distribution, for both the fundamental and overtone CH stretch modes, at 15 eV while at 20, 30, and 40 eV, the cross sections once again become somewhat more forward peaked in magnitude at the smaller scattered electron angles. In our recent elastic electron scattering and total cross section paper on phenol,[21] we found that at least for intermediate energies, it was profitable to compare the electron–phenol to the electron–benzene cross section results. It therefore makes sense to also consider such a comparison for vibrational excitation. Unfortunately, absolute electron impact vibrational scattering cross sections for benzene are also scarce, with the only data known to us being an excitation function measurement between 1 and 30 eV, for a scattered electron angle of 90° and for an energy loss (ΔE) of 0.380 eV from Kato *et al.*[33] Hence that energy loss corresponds (see Fig. 1) to our CH stretch + combination modes. While the excitation function measurement of Kato *et al.* does exhibit some scatter, we can estimate the benzene vibrational DCS for that mode to be

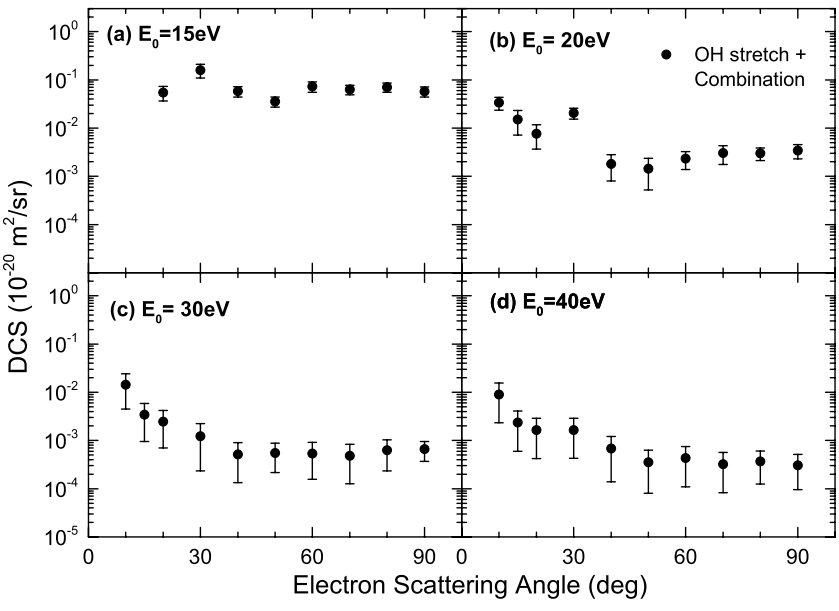

FIG. 4. Differential cross sections ($\times 10^{-20}$ m^2/sr) for electron impact excitation of the unresolved OH stretch and combination modes (•) of phenol at various incident electron energies of (a) 15 eV, (b) 20 eV, (c) 30 eV, and (d) 40 eV. The energy loss range of these modes is 0.42–0.62 eV (see Fig. 1).

DCS (15 eV, 90°) ≈ 20×10^{-23} m^2/sr, DCS (20 eV, 90°) ≈ 10×10^{-23} m^2/sr, and DCS (30 eV, 90°) ≈ 4×10^{-23} m^2/sr with the uncertainties on those data being ~30%. If we compare those results to our corresponding phenol cross sections in Table III, then we find excellent agreement between the phenol and benzene results at 20 eV and 30 eV but, at first glance, a significant discrepancy between them (~factor of 8.5) at 15 eV (the phenol DCS has a much larger magnitude). This difference might readily be explained if there was a resonance in phenol at around 15 eV that was not present in benzene. Considering the benzene vibrational excitation function spectrum and total cross section data in Kato *et al.*,[33] there is no evidence for a higher-lying resonance at around 15 eV. On the other hand, in our earlier SMC calculation, at the static exchange plus polarisation (SEP) level,[18] a clear structure in the elastic integral cross section, between ~10 and 20 eV, is found for phenol. This structure also persists in our more recent, more sophisticated, study from da Costa *et al.*[21] and, even with the coarse energy grid of their measurements, is also apparent in the experimental total cross section results of da Costa *et al.*[21] Hence, we believe that the observed discrepancy, between the present phenol CH stretch + combination mode at 90° and 15 eV, and that of Kato *et al.*[33] for the ΔE = 0.380 eV mode in benzene, is at least in part due to a higher-lying resonance (unclassified as yet) existing in phenol, and decaying into its vibrational modes, that is not present in benzene.

Finally, in Fig. 4, we plot the present DCSs for electron impact excitation of the unresolved OH stretch + combination modes in phenol. Note that the data embodied in these plots are listed in Table IV. All the points we made in relation to Figs. 2 and 3 are equally valid here for this band; namely, the magnitude of those DCSs at 15 eV, vis à vis 20, 30, and 40 eV, suggests a possible resonance enhancement of the 15 eV data and that while the angular distribution at 15 eV is quasi-isotropic, the more forward peaked nature of the higher energy cross sections suggests an influence of the target dipole moment and/or dipole polarisability on the scattering dynamics at those higher energies.

IV. CONCLUSIONS

We have reported on differential cross section measurements for electron impact excitation of some of the composite (unresolved) vibrational modes in C_6H_5OH. The energy range of those experiments was 15–40 eV, while the scattered electron angular range was 10–90°. The present results appear to be original, there being no other data or theoretical results currently in the literature against which we could compare. Certainly, we hope that our present investigation will stimulate more interest from our theoretical and experimental colleagues to study this important scattering system. One of the main aims of this work was to at least make a start on building a data base that could be used in trying to better understand the action of atmospheric plasmas on biomass and, in particular, overcoming the natural recalcitrance of biomass through plasma treatment. While we have made a beginning on fulfilling that aim, much work still needs to be done. Specifically, in the modelling of many phenomena,[1–7] it is the integral cross sections rather than the differential cross sections that are the more crucial quantities. As a consequence, we therefore foreshadow deriving integral vibrational excitation cross sections from the present data. In addition, the earlier elastic scattering SMC-SEP computation of de Oliveira *et al.*[18] clearly identified three lower-lying (in terms of energy) shape resonances that impacted significantly on the energy dependence of that cross section. In all likelihood, those same resonances might well also decay into the open vibrational excitation channels. Therefore, any attempt to extrapolate the behaviour of the present cross sections from 15 eV to their respective thresholds, e.g., using linear or cubic spline functions, is bound to be in error with actual measurements (or accurate theory) for those cross sections being required.

ACKNOWLEDGMENTS

This research was supported by the Australian and Brazilian Governmental Funding Agencies (ARC, CNPq and CAPES). D.B.J. thanks the ARC for a Discovery Early Career Researcher Award. R.F.C.N. acknowledges CNPq and Flinders University for financial assistance, while M.J.B. thanks CNPq for his "Special Visiting Professor" award. E.M.O., R.F.C., M.T.N.V., and M.A.P.L. acknowledge financial support from FAPESP, while R.F.C., M.T.N.V., M.H.F.B., M.C.A.L., and M.A.P.L. acknowledge financial support from CNPq. K.L.N. also thanks CNPq for an "Attracting Young Talent" grant under the Science Without Borders program.

[1]L. Campbell and M. J. Brunger, Plasma Sources Sci. Technol. **22**, 013002 (2013).
[2]M. C. Fuss, A. G. Sanz, A. Muñoz, F. Blanco, M. J. Brunger, S. J. Buckman, P. Limão-Vieira, and G. García, Appl. Radiat. Isot. **83**, 159 (2014).
[3]R. D. White, W. Tattersall, G. Boyle, R. E. Robson, S. Dujko, Z. Lj. Petrovic, A. Bankovic, M. J. Brunger, J. P. Sullivan, S. J. Buckman, and G. Garcia, Appl. Radiat. Isot. **83**, 77 (2014).
[4]N. A. Garland, M. J. Brunger, G. Garcia, J. de Urquijo, and R. D. White, Phys. Rev. A **88**, 062712 (2013).
[5]R. D. White, M. J. Brunger, N. A. Garland, R. E. Robson, K. F. Ness, G. García, J. de Urquijo, S. Dujko, and Z. Lj. Petrović, Eur. Phys. J. D **68**, 125 (2014).
[6]K. F. Ness, R. E. Robson, M. J. Brunger, and R. D. White, J. Chem. Phys. **136**, 024318 (2012).
[7]J. de Urquijo, E. Basurto, A. M. Juárez, K. F. Ness, R. E. Robson, M. J. Brunger, and R. D. White, J. Chem. Phys. **141**, 014308 (2014).
[8]M. J. Brunger and S. J. Buckman, Phys. Rep. **357**, 215 (2002).
[9]E. H. Bjarnason, F. H. Ómarsson, M. Hoshino, H. Tanaka, M. J. Brunger, P. Limão-Vieira, and O. Ingólfsson, Int. J. Mass Spectrom. **339-340**, 45 (2013).
[10]F. H. Ómarsson, B. Reynisson, M. J. Brunger, M. Hoshino, H. Tanaka, P. Limão-Vieira, and O. Ingólfsson, Int. J. Mass Spectrom. **365-366**, 275 (2014).
[11]S. Engmann, M. Stano, P. Papp, M. J. Brunger, Š. Matejčík, and O. Ingólfsson, J. Chem. Phys. **138**, 044305 (2013).
[12]L. Campbell, M. J. Brunger, Z. L. Petrovic, M. Jelisavcic, R. Panajotovic, and S. J. Buckman, Geophys. Res. Lett. **31**, L10103, doi:10.1029/2003GL019151 (2004).
[13]T. P. T. Do, H. V. Duque, M. C. A. Lopes, D. Konovalov, R. D. White, M. J. Brunger, and D. B. Jones, J. Chem. Phys. **142**, 124306 (2015).
[14]H. V. Duque, T. P. T. Do, M. C. A. Lopes, D. Konovalov, R. D. White, M. J. Brunger, and D. B. Jones, J. Chem. Phys. **142**, 124307 (2015).
[15]H. V. Duque, L. Chiari, D. B. Jones, Z. Pettifer, G. B. da Silva, P. Limão-Vieira, F. Blanco, G. García, R. D. White, M. C. A. Lopes, and M. J. Brunger, J. Chem. Phys. **140**, 214306 (2014).
[16]J. Amorim, C. Oliveira, J. A. Souza-Corrêa, and M. A. Ridenti, Plasma Processes Polym. **10**, 670 (2013).
[17]E. M. de Oliveira, R. F. da Costa, S. d'A. Sanchez, A. P. P. Natalense, M. H. F. Bettega, M. A. P. Lima, and M. T. do N. Varella, Phys. Chem. Chem. Phys. **15**, 1682 (2013).

[18]E. M. de Oliveira, S. d'A. Sanchez, M. H. F. Bettega, A. P. P. Natalense, M. A. P. Lima, and M. T. do N. Varella, Phys. Rev. A **86**, 020701(R) (2012).
[19]D. B. Jones, G. B. da Silva, R. F. C. Neves, H. V. Duque, L. Chiari, E. M. de Oliveira, M. C. A. Lopes, R. F. da Costa, M. T. do N. Varella, M. H. F. Bettega, M. A. P. Lima, and M. J. Brunger, J. Chem. Phys. **141**, 074314 (2014).
[20]G. B. da Silva, R. F. C. Neves, L. Chiari, D. B. Jones, E. Ali, D. H. Madison, C. G. Ning, K. L. Nixon, M. C. A. Lopes, and M. J. Brunger, J. Chem. Phys. **141**, 124307 (2014).
[21]R. F. da Costa, E. M. de Oliveira, M. H. F. Bettega, M. T. do N. Varella, D. B. Jones, M. J. Brunger, F. Blanco, R. Colmenares, P. Limão-Vieira, G. García, and M. A. P. Lima, J. Chem. Phys. **142**, 104304 (2015).
[22]R. F. C. Neves, D. B. Jones, M. C. A. Lopes, K. L. Nixon, G. B. da Silva, H. V. Duque, E. M. de Oliveira, R. F. da Costa, M. T. do N. Varella, M. H. F. Bettega, M. A. P. Lima, K. Ratnavelu, G. García, and M. J. Brunger, J. Chem. Phys. **142**, 104305 (2015).
[23]M. W. Schmidt *et al.*, J. Comput. Chem. **14**, 1347 (1993).
[24]M. J. Brunger and P. J. O. Teubner, Phys. Rev. A **41**, 1413 (1990).
[25]T. P. T. Do, M. Leung, M. Fuss, G. Garcia, F. Blanco, K. Ratnavelu, and M. J. Brunger, J. Chem. Phys. **134**, 144302 (2011).
[26]Z. Mašín, J. D. Gorfinkiel, D. B. Jones, S. M. Bellm, and M. J. Brunger, J. Chem. Phys. **136**, 144310 (2012).
[27]D. B. Jones, S. M. Bellm, F. Blanco, M. Fuss, G. García, P. Limão-Vieira, and M. J. Brunger, J. Chem. Phys. **137**, 074304 (2012).
[28]L. Chiari, H. V. Duque, D. B. Jones, P. A. Thorn, Z. Pettifer, G. B. da Silva, P. Limão-Vieira, D. Duflot, M.-J. Hubin-Franskin, J. Delwiche, F. Blanco, G. García, M. C. A. Lopes, K. Ratnavelu, R. D. White, and M. J. Brunger, J. Chem. Phys. **141**, 024301 (2014).
[29]M. Allan, J. Phys. B **38**, 3655 (2005).
[30]H. Cho, R. J. Gulley, K. Sunohara, M. Kitajima, L. J. Uhlmann, H. Tanaka, and S. J. Buckman, J. Phys. B **34**, 1019 (2001).
[31]R. J. Gulley and S. J. Buckman, J. Phys. B **32**, L405 (1999).
[32]See http://cccbdb.nist.gov/ for dipole polarisability and IR absorption spectrum of phenol.
[33]H. Kato, S. Kobayashi, C. Makochekanwa, M. Hoshino, N. Shinohara, O. Sueoka, H. Cho, and H. Tanaka, Phys. Rev. A **79**, 062702 (2009).